Supporting Information

Production of Extended Single-Layer Graphene

Mingsheng Xu[†‡*], Daisuke Fujita[§⊥], Keisuke Sagisaka[§], Eiichiro Watanabe[∥], Nobutaka Hanagata[∥δ]

[†] International Center for Young Scientists, National Institute for Materials Science, 1-2-1 Sengen, Tsukuba, Ibaraki 305-0047, Japan

[‡] MOE Key Laboratory of Macromolecule Synthesis and Functionalization, State Key Laboratory of Silicon Materials, and Department of Polymer Science and Engineering, Zhejiang University, Hangzhou 310027, P. R. China

[§] Advanced Nano Characterization Center, National Institute for Materials Science, 1-2-1 Sengen, Tsukuba, Ibaraki 305-0047, Japan

[⊥] International Center for Materials Nanoarchitectonics, National Institute for Materials Science, 1-2-1 Sengen, Tsukuba, Ibaraki 305-0047, Japan

[∥] Nanotechnology Innovation Center, National Institute for Materials Science, 1-2-1 Sengen, Tsukuba, Ibaraki 305-0047, Japan

[δ] Graduate School of Life Science, Hokkaido University, Sapporo, Japan

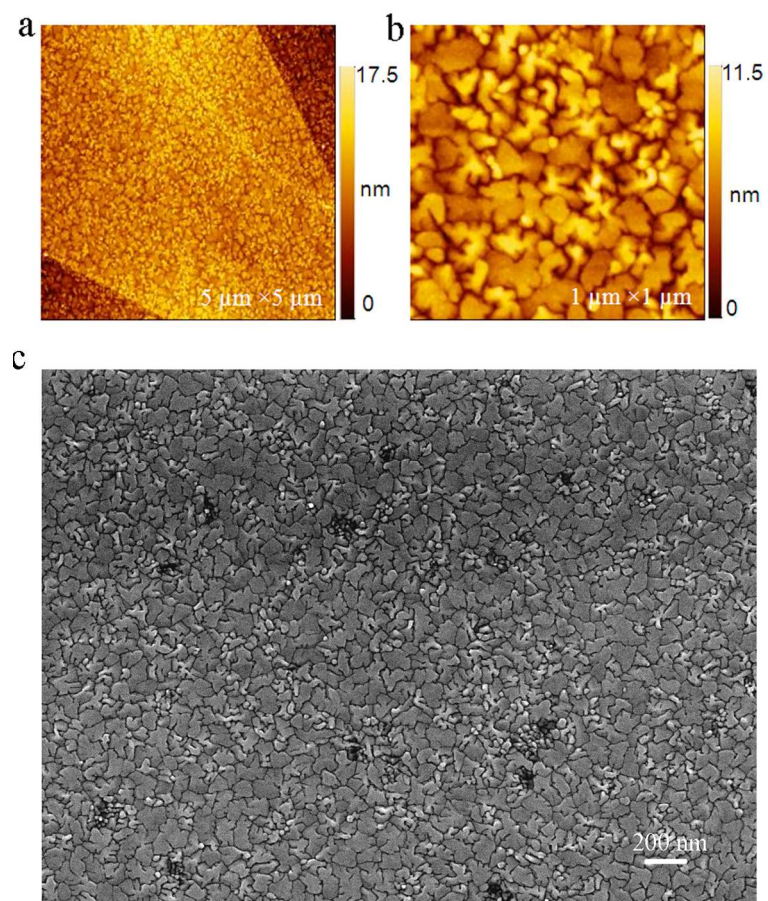*Corresponding author: msxu@zju.edu.cn; XU.Mingsheng@nims.go.jp

Figure S1 Characterization of as-grown 100 nm Ni on HOPG(0001) substrate. (a)-(b) AFM images. (c) SEM image obtained with an acceleration voltage of 20 kV.
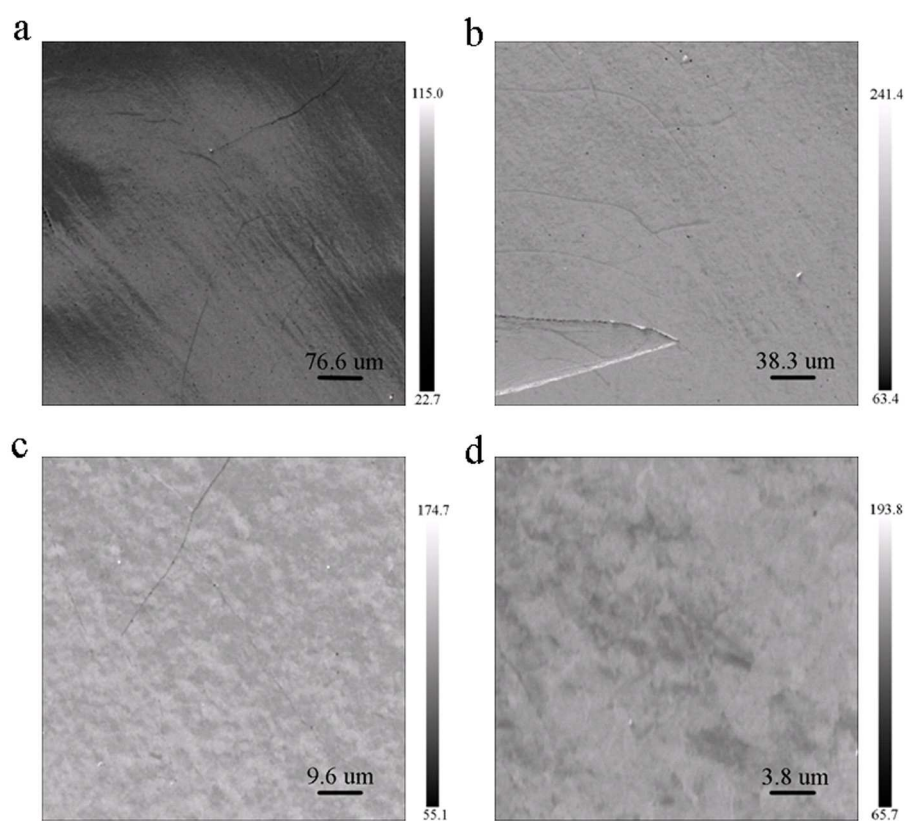
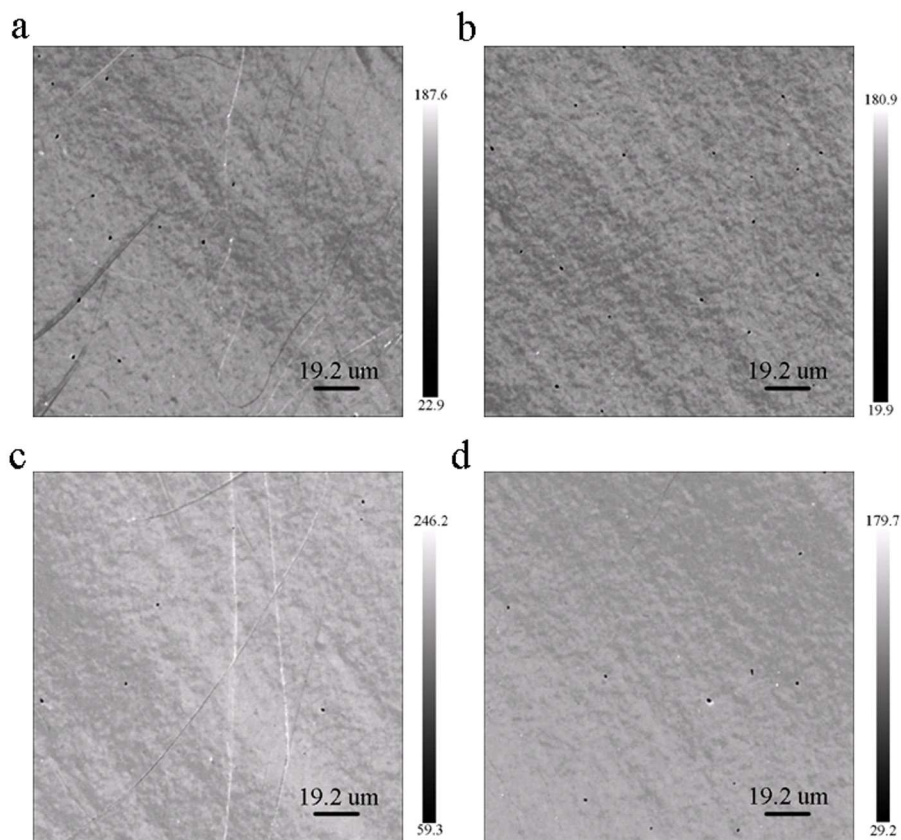**Figure S2.** Typical SEM images of graphene sheet on Ni(111)/HOPG(0001).

Figure S3. Typical SEM images of graphene sheet on Ni(111)/HOPG(0001).

Results shown in Fig. 2 and Fig. S2-3 were obtained from a same sample. The SEM images in Figs. S2-S3 show typical topographic features of our graphene sheet on Ni(111)/HOPG(0001), including bright and dark grains, grain boundaries, steps, hole-like defects, and bright protrusions. We used the above images together with AES spectra to analyze defects in our graphene sheet on Ni(111)/HOPG(0001). We calculated the defect area of hole-like defects and wide grain boundaries where the graphene film appeared to be non-continuous.

Discussion of orientation deviation of Ni grains covered with graphene (Fig. S4)

The SEM images in Fig. 2a and Fig. S2-3 show color contrast, but the intensity of the C KLL AES spectra shows no change with sample regions (Fig. 2g), in contrast to the intensity of the Ni LMM AES spectra (Fig. 2h). Thus, the contrast in the SEM image resulted mostly from different electron emissions of Ni grains. Differences in electron emissions are believed to be due to different orientations of Ni grains, and different intensities of Ni LMM transition may be due to channeling effects stemming from different orientations. To provide evidence of orientation deviation from the Ni(111) direction, we probed the crystal orientation of the Ni surface on HOPG(0001) covered with our graphene sheet using EBSD in a field-emission SEM system. The apparently large grains observed in the SEM image (Fig. S4a) were revealed to consist of many small grains (Fig. S4b) with different orientations (Fig. S4e). In the case of the Ni surface annealed for ~23 h at 650 °C, the crystal orientation of all grains is seemingly in the Ni(111) direction, as shown in Fig. S4b-c. However, with respect to the Ni(111) direction (Fig. S4e-g), 72.5% of grains were oriented in a range from 0° to 1°, 26.7% of grains were in a range from 1° to 2°, and 0.7% were in a range from 2° to 3°.

Electron backscattered diffraction (EBSD): EBSD analysis of the crystallographic orientation of the Ni grains covered with graphene was carried out using a JSM-7001F field-emission scanning electron microscopy (SEM) system with an accelerating voltage of 15-20 kV.
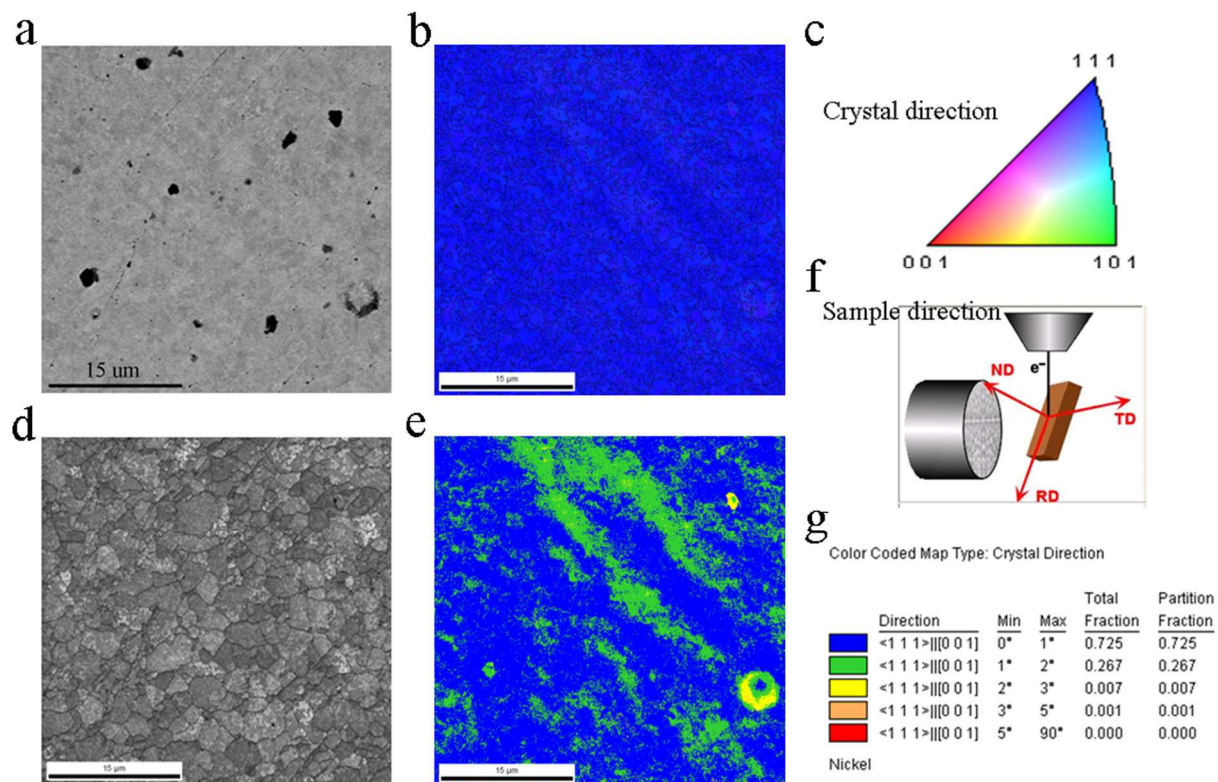
Figure S4. Electron backscatter diffraction analysis of crystallographic orientation of a Ni film treated for ~23 h at 650 ℃. scale bar in (a), (b), (c), (d) is 15 µm. (a) SEM image, showing large grains. (b)-(c) Inverse pole <h k l> map plus grain boundaries in the sample direction of [RD TD ND] = [001], indicating that all grains seem to be in the (111) orientation. The boundary is defined when the rotation angle of neighboring grains exceeds 2°; only the boundaries with rotation angles within 15° of 180° (fraction of 0.895) were shown. (d) Crystal quality with Kikuchi pattern analysis, corresponding to the image in (a). (e)-(g) Crystal disorientation chart with respect to the Ni(111) direction. (f) Sample direction of the measurement.
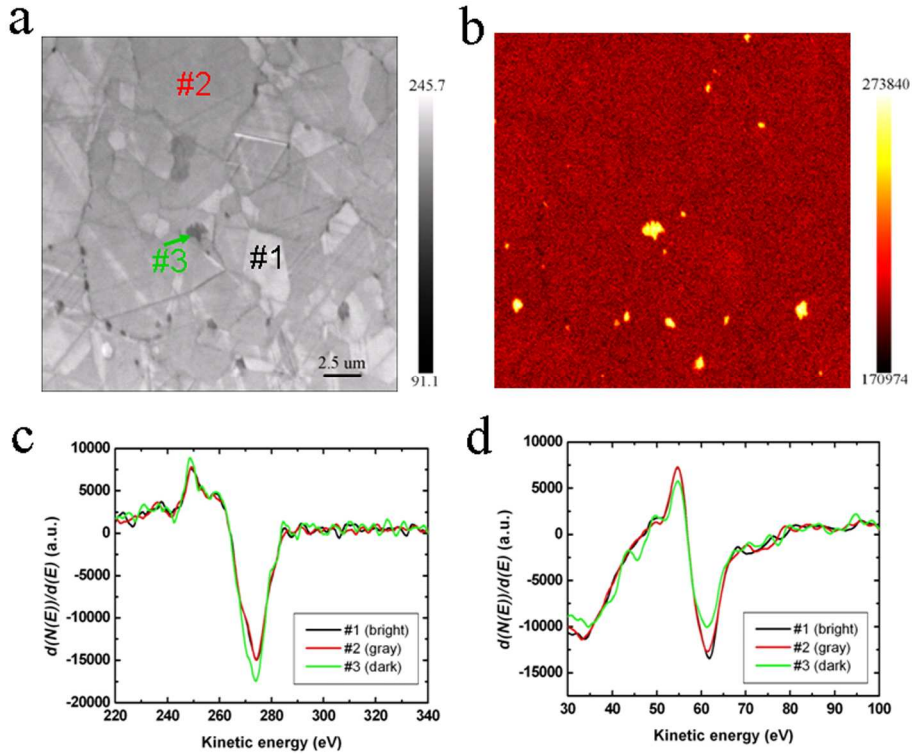
Figure S5. AES characterization of graphene sample synthesized on Ni(111)/HOPG(0001) with annealing time of ~18 h at 900 ℃. (a) SEM image. (b) corresponding C KLL Auger electron map, showing excessive carbon precipitation at grain boundaries. (c) C KLL AES differential spectra obtained from the marked regions in (a). (d) Ni MVV AES differential spectra. The spectra and maps suggest a thicker graphene film at grain boundaries. However, the Auger electron intensities obtained in the dark and bright regions are identical. The results suggest that an increase in the treatment temperature and prolonged time may lead to more hole-like defects, widening of the gaps between grains, and non-uniform thickness of graphene layer.
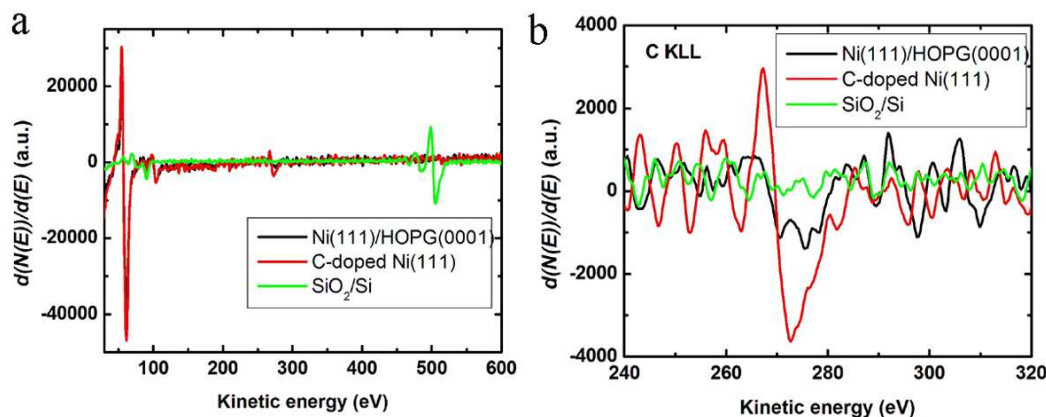
Figure S6. Comparison of carbon content in our Ni(111) template diffused from HOPG(0001), in carbon-doped Ni(111), and absorbed in SiO$_2$/Si. The AES spectra were obtained at the same experimental conditions. (a) Survey AES spectra. (b) C KLL AES spectra. The spectrum marked with "Ni(111)/HOPG(0001) represents that was obtained after 700 s sputtering our graphene sample synthesized on Ni(111)/HOPG(0001); the spectrum marked with "C-doped Ni(111)" represents that was obtained after 700 s sputtering a Ni(111) sample that had been doped with carbon[1] at 650 ℃ for 20 h; the spectrum marked with "SiO$_2$/Si" represents that was obtained from a clean SiO$_2$/Si sample (without sputter). The peak-to-peak magnitude ratio of the C KLL signal between our Ni(111)/HOPG(0001) and the C-doped Ni(111) is 0.21. The results suggest the following two points. (1) The carbon absorbed in the SiO$_2$/Si is negligible, suggesting the free carbon in our AES system has little contribution to our AES measurement; and (2) the carbon content in our Ni(111) substrate diffused from the HOPG(0001) is significantly lower than that in the carbon-doped Ni(111), *i.e*, the saturation solubility of carbon in Ni(111) at the temperature. The saturation solubility of carbon in Ni at 650 °C is less than 0.1% in weight.[2]
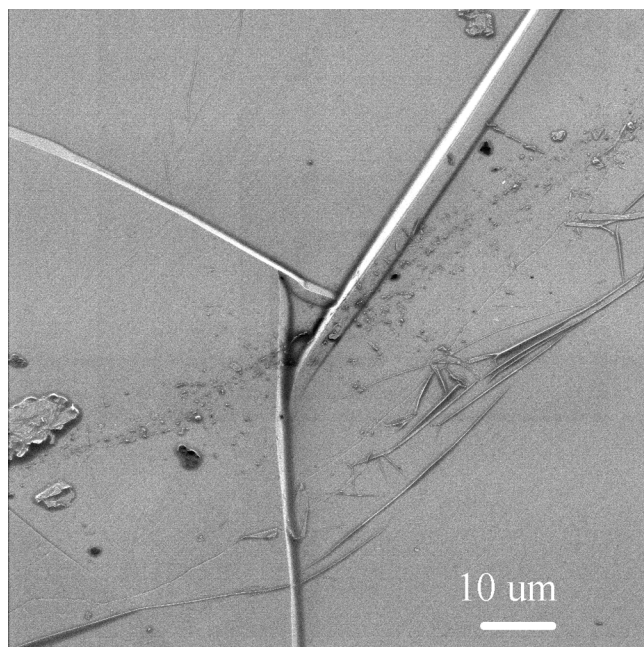
Figure S7. Helium ion micrograph of our graphene on Ni/HOPG, showing large-scale terraces, steps as well as debris. The image was obtained by ZEISS Orion helium ion microscope, operated at 35 kV acceleration voltage and with a beam current of 0.4 pA.

Graphene film grown on Ni/SiO$_2$/Si substrate (Fig. S8)

For a comparison, we have also synthesized graphene films on Ni/SiO$_2$/Si substrate by a CVD method, giving rise to graphene films with a mixture of different numbers of graphene layers that showed a non-uniform C KLL map and peak intensity.
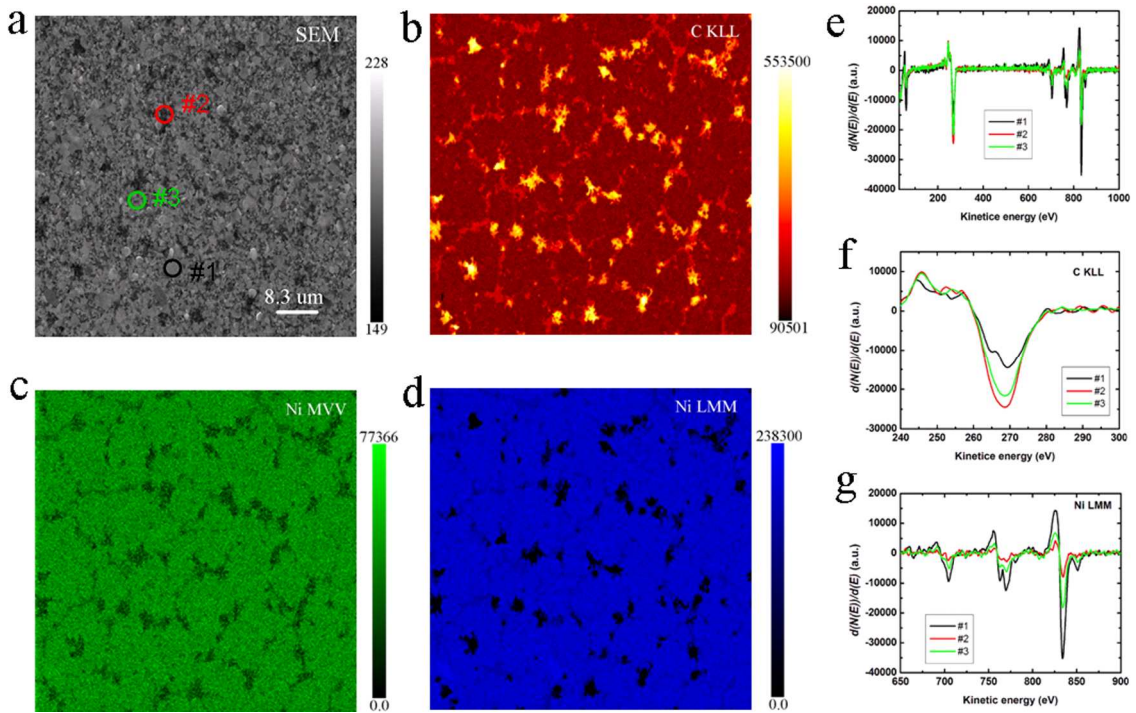

Figure S8. AES characterization graphene film synthesized on Ni/SiO$_2$/Si substrate by chemical vapor deposition method. (a) SEM image. (b) C KLL Auger electron map. (c) Ni MVV Auger electron map. (d) Ni LMM Auger electron map. (e)-(g) AES differential spectra of the graphene film obtained from the regions marked with corresponding colored circles in (a). (e) Survey spectra. (f) C KLL spectra. (g) Ni LMM spectra. The results suggest that the thickness of the graphene film synthesized on Ni/SiO$_2$/Si is different in different sample regions, and suggest the advantage of our Ni/HOPG system for production of graphene.

References

1. Gao, J. H.; Fujita, D.; Xu, M. S.; Onishi, K.; Miyamoto, S. Unique synthesis of few-layer graphene films on carbon-doped Pt83Rh17 surface. *ACS Nano* **2010**, *4*, 1026-1032.

2. Ohtani, H.; Hasebe, M.; Nishizawa, T. Calculation of Fe-C, Co-C and Ni-C phase diagrams. *Trans. ISIJ* **1984**, *24*, 857-864.